

Unmanned aerial vehicle and proximal sensing of vegetation indices in olive tree (*Olea europaea*)

Eliseo Roma, Pietro Catania, Mariangela Vallone, Santo Orlando

Department of Agricultural, Food and Forest Sciences, University of Palermo, Italy

Abstract

Remote and proximal sensing platforms at the service of precision olive growing are bringing new development possibilities to the sector. A proximal sensing platform is close to the vegetation, while a remote sensing platform, such as unmanned aerial vehicle (UAV), is more distant but has the advantage of rapidity to investigate plots. The study aims to compare multispectral and hyperspectral data acquired with remote and proximal sensing platforms. The comparison between the two sensors aims at understanding the different responses their use can provide on a crop, such as olive trees having a complex canopy. The multispectral data were acquired with a DJI multispectral camera mounted on the UAV Phantom 4. Hyperspectral acquisitions were carried out with a FieldSpec® HandHeld 2™ Spectroradiometer in the canopy portions exposed to South, East, West, and North. The multispectral images were processed with Geographic Information System software to extrapolate spectral information for each cardinal direction's exposure. The three main Vegetation indices were used: normalized difference vegetation index (NDVI), normalized difference red-edge index (NDRE), and modified soil adjusted vegetation index (MSAVI). Multispectral data

could describe the total variability of the whole plot differentiating each single plant status. Hyperspectral data were able to describe vegetation conditions more accurately; they appeared to be related to the cardinal exposure. MSAVI, NDVI, and NDRE showed correlation $r=0.63^{**}$, 0.69^{**} , and 0.74^{**} , respectively, between multispectral and hyperspectral data. South and West exposures showed the best correlations with both platforms.

Introduction

Since the early 2000s, the agricultural sector has been undergoing a significant change in crop management, becoming increasingly precise and aiming at differentiating agricultural practices (irrigation, tillage, etc.) according to the variability of the field (Lal, 2015; Marin *et al.*, 2021; Zhang *et al.*, 2002). Precision farming uses different technologies capable of acquiring spatially variable information about the vegetation condition of the crops (Roma and Catania, 2022). For these purposes, many sensor types can be used, such as multispectral and hyperspectral cameras (Avola *et al.*, 2019; Deng *et al.*, 2018; Jensen, 2009; Pagliai *et al.*, 2022). Multispectral cameras can acquire a low number of spectral bands, each with a bandwidth between 10 and 40 nm. Hyperspectral cameras can acquire more comprehensive wavelength ranges with few nanometres of spectral resolution (Lu *et al.*, 2020).

Spectral data are an important source of information for identifying crop status and can be processed in different ways (Lu *et al.*, 2020). Hyperspectral data are enjoying great success given the various possible applications (Benelli *et al.*, 2020). Hyperspectral information can be processed to calculate vegetation indices (VI) (Xie *et al.*, 2014; Xue and Su, 2017) that can provide different information depending on the bands used and the equations involved. In olive growing, the most widely used indices are normalized difference vegetation index (NDVI), normalized difference red-edge index (NDRE), and modified soil adjusted vegetation index (MSAVI). NDVI and NDRE are classified as ratio VI, while MSAVI is classified as an orthogonal index (Dorigo *et al.*, 2007) based on their relation with the biomass, leaf area index (LAI), plant conditions and soil characteristics. Therefore, they can discriminate soil and non-pure pixels differently, as well as the resulting spectral information (Er-Rami *et al.*, 2021; Xue and Su, 2017). NDVI is the most widely used ratio index in olive growing and many other crops, defined by Rouse *et al.* (1974). It measures vegetation conditions using the highest absorption and reflectance regions of chlorophyll and is helpful in characterising canopy growth or vigour (Xue and Su, 2017). Its main limitation is due to the high sensitivity of background factors, such as shade, canopy and soil brightness. NDRE has a high differentiating capacity on vigorous vegetation compared to stressed vegetation (Maccioni *et al.*, 2001). This is due to the use of the RedEdge band (at about $740 \text{ nm} \pm 10$) that is highly reactive to vegetation conditions. Its

Correspondence: Mariangela Vallone, Department of Agricultural, Food and Forest Sciences, University of Palermo, viale delle Scienze ed. 4, 90128, Palermo, Italy.
Tel.: +39.9123865609. E-mail: mariangela.vallone@unipa.it

Key words: canopy; NDVI; MSAVI; NDRE; spectroradiometer.

Contributions: the authors contributed equally.

Conflict of interest: the authors declare no potential conflict of interest.

Funding: none.

Received: 4 November 2022.

Accepted: 13 February 2023.

©Copyright: the Author(s), 2023

Licensee PAGEPress, Italy

Journal of Agricultural Engineering 2023; LIV:1536

doi:10.4081/jae.2023.1536

This work is licensed under a Creative Commons Attribution-NonCommercial 4.0 International License (CC BY-NC 4.0).

Publisher's note: all claims expressed in this article are solely those of the authors and do not necessarily represent those of their affiliated organizations, or those of the publisher, the editors and the reviewers. Any product that may be evaluated in this article or claim that may be made by its manufacturer is not guaranteed or endorsed by the publisher.

main limitation is the high sensitivity of background factors, such as shade, brightness of vegetation canopies, and presence of weeds and soil. MSAVI has a high capacity of discriminating the vegetation from the ground; it was defined by (Qi *et al.*, 1994).

The multispectral data are significantly more used than hyperspectral in olive orchards. The multispectral application concerns the assessment of plant health (Álamo *et al.*, 2012; Zhang *et al.*, 2021). Indeed, in the olive orchard, the multispectral image was used to apply fertilisers (López-Granados *et al.*, 2004; Van Evert *et al.*, 2017) to obtain the biophysical characteristic of the trees (Sola-Guirado *et al.*, 2017; Solano *et al.*, 2019), to manage irrigation (Ben-Gal *et al.*, 2009; Berni *et al.*, 2009; Sghaier *et al.*, 2022; Vanella *et al.*, 2021) and pruning (Jiménez-Brenes *et al.*, 2017) and to build yield prediction models (Stateras and Kalivas, 2020).

In olive orchards, biometric information and LAI parameter were determined using hyperspectral images from remote sensing platforms such as the Quickbird satellite and the compact airborne spectrographic imager, obtaining good coefficients of determination (Gómez *et al.*, 2011). Other applications of hyperspectral data concerned the nutritional status determination for nitrogen (N) and potassium (K) elements (Gómez-Casero *et al.*, 2007). Good results have been obtained from aircraft and hyperspectral data to investigate water status (Sepulcre-Cantó *et al.*, 2005, 2006), yield and fruit quality (Sepulcre-Cantó *et al.*, 2007).

However, few studies have tried to compare multispectral and hyperspectral data in agriculture. For instance, Mariotto *et al.* (2013) compared Hyperion hyperspectral imagery to Landsat multispectral imagery for the estimation of crop productivity and the classification of crop types. The authors reported better results using hyperspectral imagery than using Landsat imagery. Previous studies have also demonstrated the superior performance of hyperspectral over multispectral images in monitoring vegetation properties, such as estimating leaf area index (Lee *et al.*, 2004), discriminating crop types (Nigam *et al.*, 2019), retrieving crop biomass (Marshall and Thenkabail, 2015), and assessing leaf nitrogen content (Sun *et al.*, 2017). Multispectral cameras are increas-

ingly associated with remote acquisition platforms such as Unmanned aerial vehicle (UAV). In contrast, spectroradiometers are used with proximal platforms because hyperspectral sensors have a higher sensitivity to noise in the signal acquisition that could compromise the final result (Transon *et al.*, 2018). Despite this, few studies compared multispectral and hyperspectral data acquired from two platforms without the same point of view (POV) and viewing angle. This can result in different spectral information about the crop. The study aimed to apply remote and proximal sensors to describe the canopy condition of an olive growing through different VI. The comparison between the two sensors was carried out to understand the different responses their use can provide on a crop such as olive trees, having a complex canopy made up of sprouts with both assurgent and procumbent growth typical of the vase shape growing system. A UAV was used for remote sensing through a multispectral camera, while a hand-held spectroradiometer was used for proximal sensing with a hyperspectral camera. In particular, the goal was to verify whether multispectral images acquired from a remote UAV platform at 50 m above ground level and hyperspectral data acquired from proximal platforms can describe the same vegetation conditions of olive trees using three different VI.

Materials and Methods

Study area

The field test is located in Calatafimi-Segesta (Trapani, Italy) with coordinates Lat 37°51'48.21 "N; Long 12°57'15.17 "E (World Geodetic Coordinate System 1984; Figure 1). According to Koppen-Geiger's classification, the area's climate is Csa (Mediterranean hot summer climates; Kottek *et al.*, 2006). Climatic data recorded from 1985 to 2011 showed a mean annual air temperature ranging from 16.1 to 18.6°C and a mean annual precipitation ranging from 440 to 495 mm (Sicilian agrometeoro-

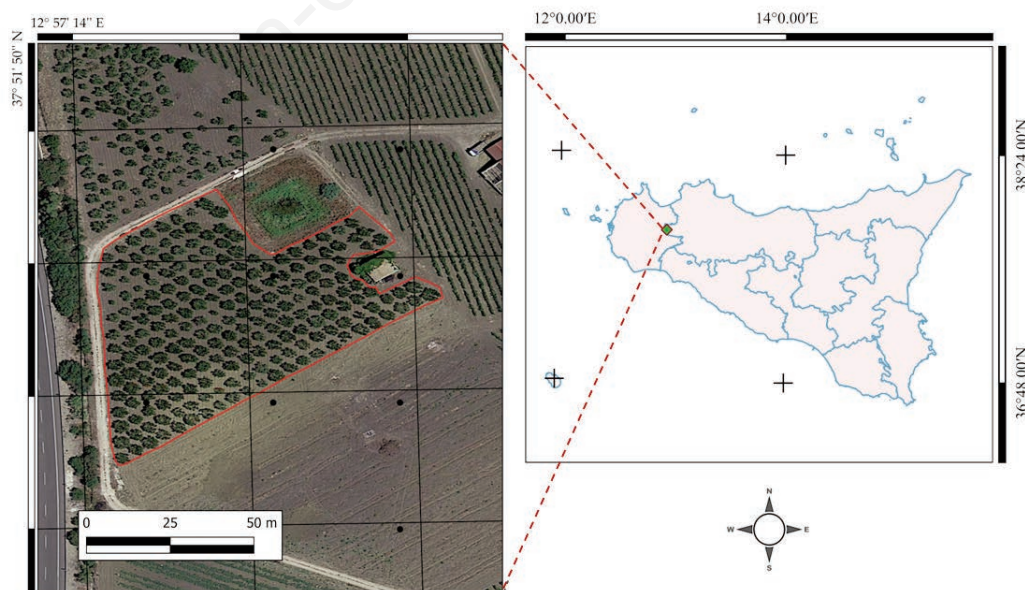


Figure 1. a) Plot study area; b) Experimental site location.

logical information service). The soil moisture regime is xeric, the border with the aridic one, and the thermic temperature regime.

The experiment was carried out in 2021 in an olive orchard cultivated according to the ordinary management practices of the area without irrigation.

The field has an area of 5860 m², with a flat surface topography. The soil presents a low percentage of coarse fragments on most of the surface. According to the United States Department of Agriculture classification, the soil belongs to the Franco-Sandy-Argillaceous granulometric class. The olive grove was planted in 2002 with cv. Cerasuola, a single cultivar typical of the area and at the time of the experimentation. The olive grove is trained in a vase shape, with a vertical trunk about 0.90 m high from the ground and with three-four main branches. The layout of the plant is 5.00'5.50 m. It is a typical farming system for the olive tree defined as "traditional". During the experimental season, all plants were in production (on-year). The plant had a traditional trelling system with a layout of 5.0'5.5 m, and the total number of trees considered in the tests was 211. Twenty-four plants were randomly selected for the multispectral and hyperspectral acquisition. The direction of the rows is NE-SW at an angle of 60° to the North.

Instrumentation used

Multispectral data acquisition was performed using a Phantom4 Multispectral drone (DJI, Shenzhen, China), a high-precision drone with a seamlessly integrated multispectral imaging system. The multispectral camera has six 1/2.9" CMOS sensors: an RGB sensor for visible light imaging and five monochrome sensors for multispectral imaging with a final resolution of 2.08 MP. The monochromatic bands are Blue (B), Green (G), Red (R), Red-Edge (RE), and Near infrared (NIR), respectively, with the following central wavelengths: 450 nm, 560 nm, 650 nm, 730 nm, and 840 nm. The bandwidth sensitivity for R, G, B, and RE bands are ±16 nm and ±26 nm for the NIR band. The lens has a 62.7° field of view (FOV), a 5.74 mm focal length, and an aperture of f/2.2. The maximum final image size is 1600×1300 pixels.

The UAV was equipped with four rotors (quadcopter) with a rotary wing capable of autonomously flying over the predetermined route. It had a solar irradiance sensor on the top, allowing it to obtain pre-calibrated images. In addition, it was able to fix the exact position of the images using the exchangeable image file

data information of each image. The positioning system consisted of a multi-frequency global navigation satellite system (GNSS) capable of receiving and decoding signals from the satellites constellation NAVSTAR (GPS), GLONASS, BeiDou and Galileo, respectively, in the bands L1/L2, L1/L2, B1/B2, and E1/E5 with real time kinematic (RTK) correction (accuracy <2 cm).

The FieldSpec® HandHeld 2™ Spectroradiometer (HHS) was used to acquire hyperspectral data. The HHS is a handheld spectroradiometer that makes fast, accurate, non-destructive, non-contact measurements, operating in the spectral range from 325 to 1075 nm, with ±1 nm accuracy and a spectral resolution <3 nm at 700 nm and a radiometric resolution at 16 bits. A square section and 25° FOV determine the geometric resolution of the acquisition area. It acquires high signal-to-noise ratio spectra in less than one second using a low light dispersion grating, an integrated shutter, DriftLock dark current compensation and second-order filtering. In addition, the HHS has a colour LCD display, built-in computing capability, large internal data memory (2,000 measurements), laser pointer and GNSS input compatibility.

Flight scheduling and multispectral data acquisition

A remote UAV platform with a multispectral camera was used to obtain multispectral data. The flight mission was planned using DJI GS Pro software to set the flight parameters (height, speed, direction, etc.) and the acquisition parameters of the cameras (sequence of shots, front and lateral overlapping, etc.). In order to minimise disturbing elements such as shadows and weeds, the flight was carried out on the day of the year 217 at 12:00, with the sun rising at the zenith, after harrowing the entire plot. Before the flight, 5 ground control points (GCPs) were placed in the field, which were georeferenced using the GNSS receiver S7-G by Stonex (Italy, Milano), equipped with a Stonex geodetic antenna, already used in other experiments (Catania *et al.*, 2019, 2020). This instrument can use multiband signals from the main GNSS satellites such as GPS, GLONASS, Galileo and Bei Dou, and improve accuracy through the RTK differential correction data. The coordinates of the different GCPs were acquired in RTK mode as an average of 60 measurements. Once the GCPs were positioned, the flight proceeded under clear sky conditions and low wind speed, with the automatic guide following the set route and waypoints (Figure 2).



Figure 2. a) Drone view; b) Flight plan.

The flight was carried out at an altitude of 50 m above ground level, using RTK differential corrections, obtaining a ground sample surface of 2.6 cm. The image acquisition was performed at an average speed of $10 \text{ m} \cdot \text{s}^{-1}$ in a stop-and-go mode to minimise the distortions related to the forward speed. To get more detailed and less distorted images, the front and side overlap percentage between the image was 70%, while the gimbal pitch was set at 90° (downwards). The flight path was set to minimise flight time in specific, an angle of 178° to the North was used in our test.

Hyperspectral data acquisition

Hyperspectral acquisitions were made on 24 randomly selected plants on the same day of the flight. The measurements were carried out from 01:00 pm in the four exposures with the following sequence: South, West, North and East. Three acquisitions were realised for each exposure, and the radiometric reflectance calibration was performed using a calibrated Spectral on white reference. The acquisitions were carried out in the four lateral portions of the plants directly in the field, placing the instrument at about one meter from the canopy (Figure 3). In this way, it was possible to examine the hyperspectral information of an entire portion of the canopy without any influence of the soil for the four exposures. The acquired data were downloaded and processed through the proprietary software associated with the instrument (HH2 Sync and ViewSpec Pro). For each acquisition, the instrument output provides a specific ASCIC file (asd) that can be processed in its proprietary software, and after, it can be saved in several formats.

Unmanned aerial vehicle images pre-processing

Once the multispectral images were acquired, they were pre-processed to obtain the multiband orthomosaic. Data were processed using the Structure for motion software (Agisoft Metashape Professional version 1.7.3). This software enables photogrammetric processing of digital images and generates 3D and 2D spatial

data for use in GIS applications. Figure 4 schematically describes the workflow used for the photogrammetric processing of the different images. Once the alignment had been completed, the GCPs were inserted using the WGS84 geographical coordinate system (EPSG: 4326). Then, the identification of the GCPs on the different photos was done. The calibration of the images was made by the software, using the brightness data recorded by the brightness sensor on the drone. In addition, a white panel placed on the ground before the flight was used to complete the radiometric calibration. After constructing the Dense Cloud, it was possible to obtain the Mesh and the digital elevation model. Finally, through a process of orthorectification and mosaicking, the multiband orthomosaic was obtained (Figure 5).



Figure 3. Proximal data acquisition with the hyperspectral sensor applied on the four lateral canopy portions of the plant. The instrument was placed about one meter from the canopy.

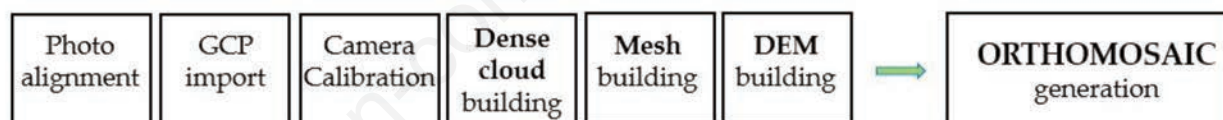


Figure 4. Workflow of photogrammetry data processing.

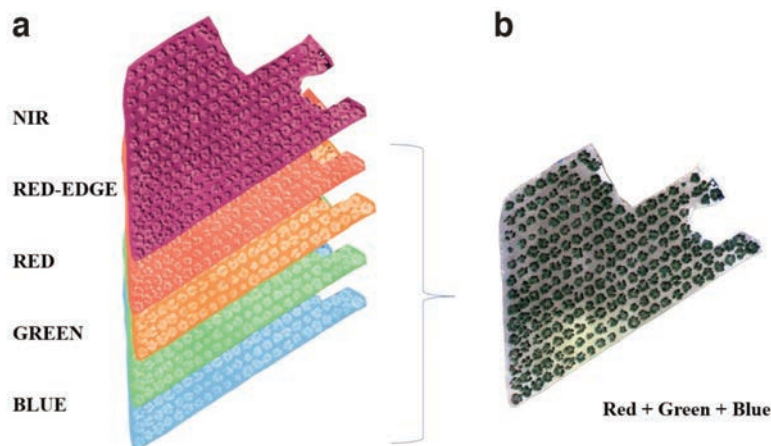


Figure 5. a) Multispectral bands; b) Orthomosaic in red, blue, and green representation.

Image processing and analysis

The orthomosaic was then processed to obtain the spectral canopy data using the open-source software QGIS version 3.16.6 Hannover (QGIS.org, 2022). The processing steps were done using the geographic object-based image analysis methodology. First, the segmentation of the image was performed in order to obtain a classification in different non-overlapping zones, starting from the VI map realised with different VI, as in Caruso *et al.* (2019). The three main VI were used: NDVI (Rouse *et al.*, 1974), MSAVI (Qi *et al.*, 1994), and NDRE (Maccioni *et al.*, 2001) (Table 1). The K-means algorithm was applied to the VI map, which allowed us to obtain a binary clustering of the image. This methodology was pre-

ferred over threshold clustering because any non-pure pixels (especially close to the canopy) could be erroneously classified as soil. This clustering algorithm was in Saga's Images analysis library.

The image segmentation for the canopy extraction was obtained by applying the following procedure (Figure 6).

Each was divided into four parts according to the exposure to the four cardinal directions. Considering that 0° is located at the centre of the North portion and turning clockwise: the North sector goes from 315° to 45°, East from 45° to 135°, South from 135° to 225° and West from 225° to 315°. The intersecting of the multi-spectral raster images with the vector of the canopy resulted in the spectral data of each plant and its four portions (Figure 7).

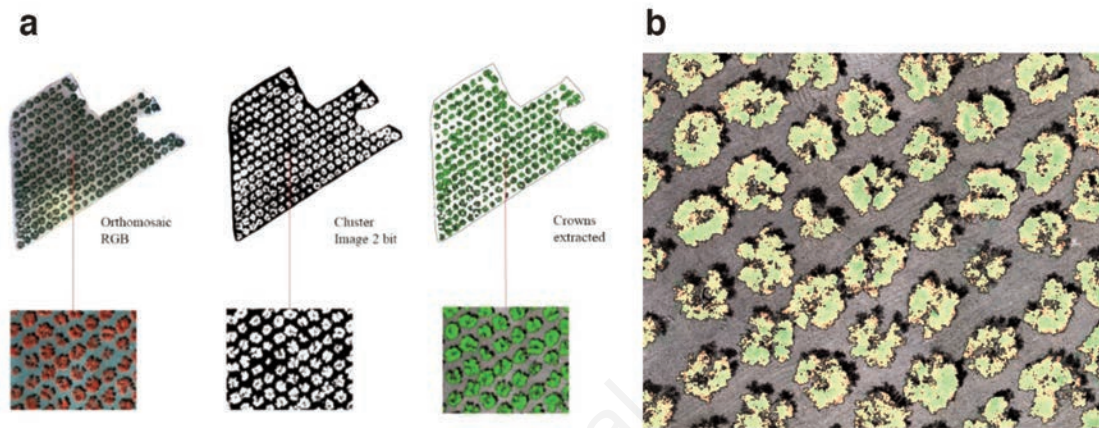


Figure 6. a) Extraction sequence of the canopy of the plants; b) Normalized difference vegetation index detail of each canopy on red, blue, and green background.

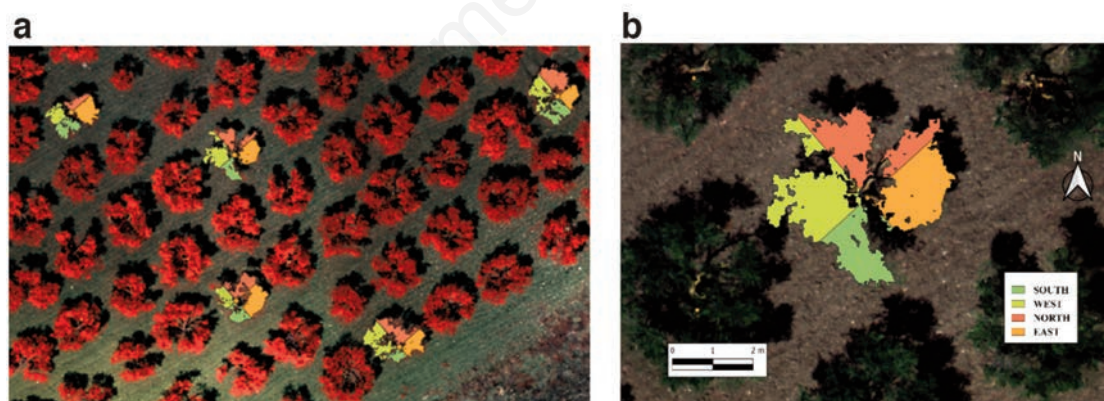


Figure 7. a) False-colour image showing the four portions of the canopy of some selected plants; b) Detail of a plant sampled for hyper-spectral measurements and the canopy divided into four portions (North, South, East, West).

Table 1. Vegetation indices used to study multispectral and hyperspectral data.

Vegetation index	Acronym	Formula	Authors
Normalized difference red-edge index	NDRE	$\frac{\rho_{Nir} - \rho_{RedEdge}}{\rho_{Nir} + \rho_{RedEdge}}$	Maccioni <i>et al.</i> , 2001
Normalized difference vegetation index	NDVI	$\frac{\rho_{Nir} - \rho_{Red}}{\rho_{Nir} + \rho_{Red}}$	Rouse <i>et al.</i> , 1994
Modified soil adjusted vegetation index	MSAVI	$\frac{[2\rho_{Nir} + 1 - \sqrt{(2\rho_{Nir} + 1)^2 - 8(\rho_{Nir} - \rho_{Red})}]}{2}$	Qi <i>et al.</i> , 1994

Statistical analysis

The VI data were subjected to analysis of variance (ANOVA) and Tukey's test to evaluate the statistical significance of the tests at a 95% confidence level. The main techniques of inferential statistics were applied using RStudio (RStudio Team, 2020) and Microsoft Excel software (Microsoft Corporation, 2018).

Results

Proximal sensing from spectroradiometer

The hyperspectral data let us to know the spectral signatures of the 24 selected plants and the reflectance of the four parts exposed at the cardinal directions (Figure 8). The average spectral signature for most of the reflectance spectra showed the typical trend of agricultural crops, with a higher reflectance in the NIR bands than in the visible region. More specifically, reflectance peaks were observed at approximately 555 nm in the green band and 770 nm in the NIR, while reflectance pits were recorded at around 690 nm. A different behaviour based on acquisition exposure was observed.

The average reflectance that characterised the sampled plants was 6.2% in the blue band, 12.3% in the green, 9.8% in the red, 41.0% in the red edge, and 61.7% in the NIR, respectively. A difference was observed between the reflectance values acquired in the different cardinal directions while maintaining the same trend along the curve.

The reflectance in the South exposure was always higher than the other three, while the North exposure showed the lowest values ($p < 0.001$). East and West exposures gave similar values; in particular, in the region between 400 and 680 nm, the West exposure shows values lower than those observed in the East exposures, whereas in the NIR region, the West exposure has, on average, significantly higher spectral reflectance values than East ($p < 0.001$).

Three VI were calculated: NDVI, NDRE, and MSAVI using the same range of the multispectral camera. Within each index, statistically significant differences were observed among the four exposures. (Table 2). In particular, the South and West exposures gave the three indices higher and significant values. Northern and Eastern exposures caused a greater dispersion of the data, especially in NDVI and MSAVI. Statistically significant differences among the indices were also observed. MSAVI gave the highest average value with a mean of 0.718 ± 0.14 followed by NDVI with

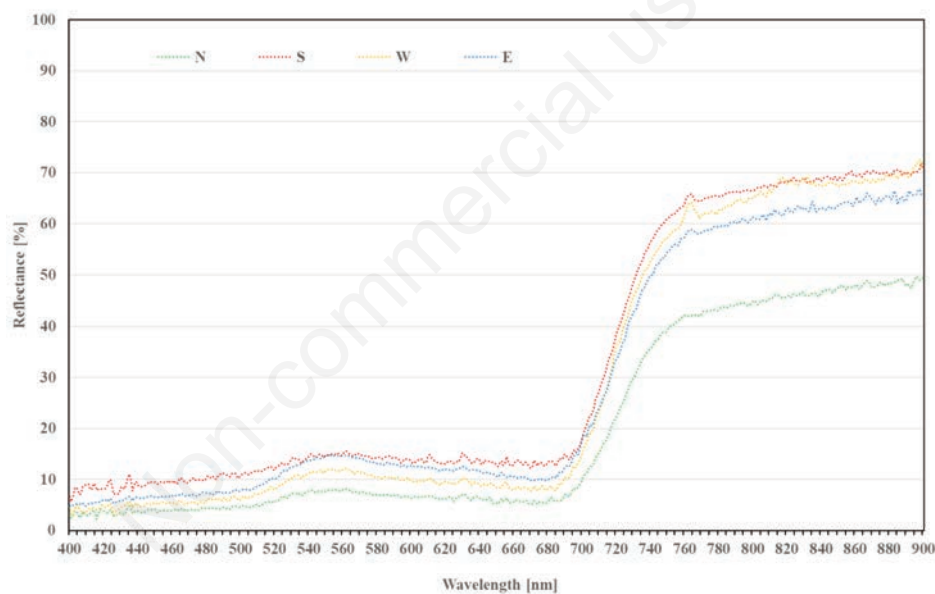


Figure 8. Representation of the reflectance of the four parts of the plants exposed at the cardinal directions (each line is the mean of 24 spectra).

Table 2. Normalized difference vegetation index, normalized difference red-edge index and modified soil adjusted vegetation index from hyperspectral data. Values are mean \pm standard deviation of the 24 selected plants.

Exposure	NDVI	NDRE	MSAVI
S	0.647 ± 0.05^a	0.170 ± 0.02^a	0.785 ± 0.04^a
W	0.643 ± 0.05^a	0.167 ± 0.02^a	0.781 ± 0.04^a
N	0.497 ± 0.15^b	0.139 ± 0.04^b	0.644 ± 0.20^b
E	0.508 ± 0.14^b	0.147 ± 0.03^{ab}	0.661 ± 0.13^b
Average	0.574 ± 0.13	0.156 ± 0.03	0.718 ± 0.14

NDVI, normalized difference vegetation index; NDRE, normalized difference red-edge index; MSAVI, modified soil adjusted vegetation index. ^{a,b}Different letters in the column indicate statistically significant differences at a significance level of 5%.

a value of 0.574 ± 0.13 and then NDRE with 0.156 ± 0.03 . The regression analysis between the indices used for the hyperspectral characterisation of the plants showed statistically significant values ($p < 0.001$) and high R^2 values. NDVI had R^2 values of 0.80 and 0.97 with NDRE and MSAVI, respectively. NDRE showed an R^2 of 0.79 with the MSAVI value. Therefore, the coefficient of determination values between the indices was very high, with statistically significant differences; the R^2 highest value was observed between MSAVI and NDVI (Figure 9).

Remote sensing from unmanned aerial vehicle

The spectral information was obtained for each tree canopy and the different exposures using the drone images. From the multispectral data, the mean values of the three VI recorded in the 24 selected plants were: 0.62 ± 0.03 , 0.53 ± 0.03 , and 0.71 ± 0.03 for NDVI, NDRE and MSAVI, respectively. No statistically significant differences were found among the mean values of the four exposures for each index (Figure 10).

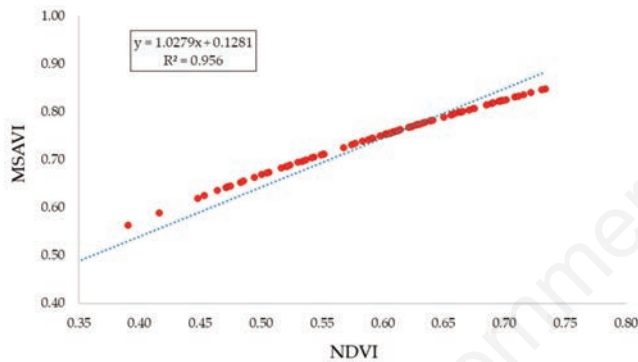


Figure 9. Linear correlation between normalized difference vegetation index and modified soil adjusted vegetation index.

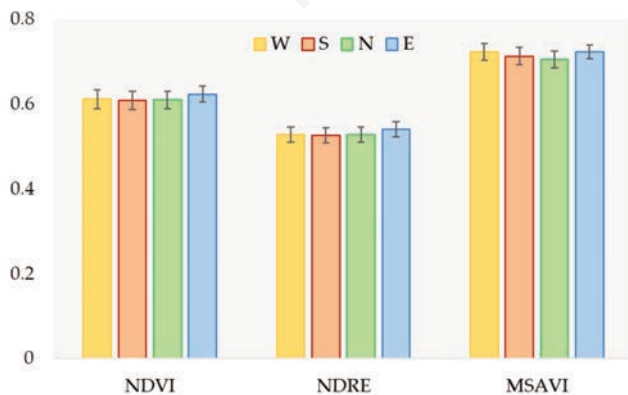


Figure 10. Normalized difference vegetation index, normalized difference red-edge index and modified soil adjusted vegetation index mean values of the individual canopies (n=24), divided into the four exposures.

The regression analysis shows that, in all the VI, the values obtained from the four exposures are statistically correlated ($p < 0.001$) to the mean value obtained per plant, with a very high coefficient of determination. In this case, the southern exposure gave the best results. In fact, the R^2 values found by comparing NDVI, NDRE and MSAVI of southern exposures with the relative mean values per plant were respectively: 0.754, 0.775 and 0.772 (Figure 11).

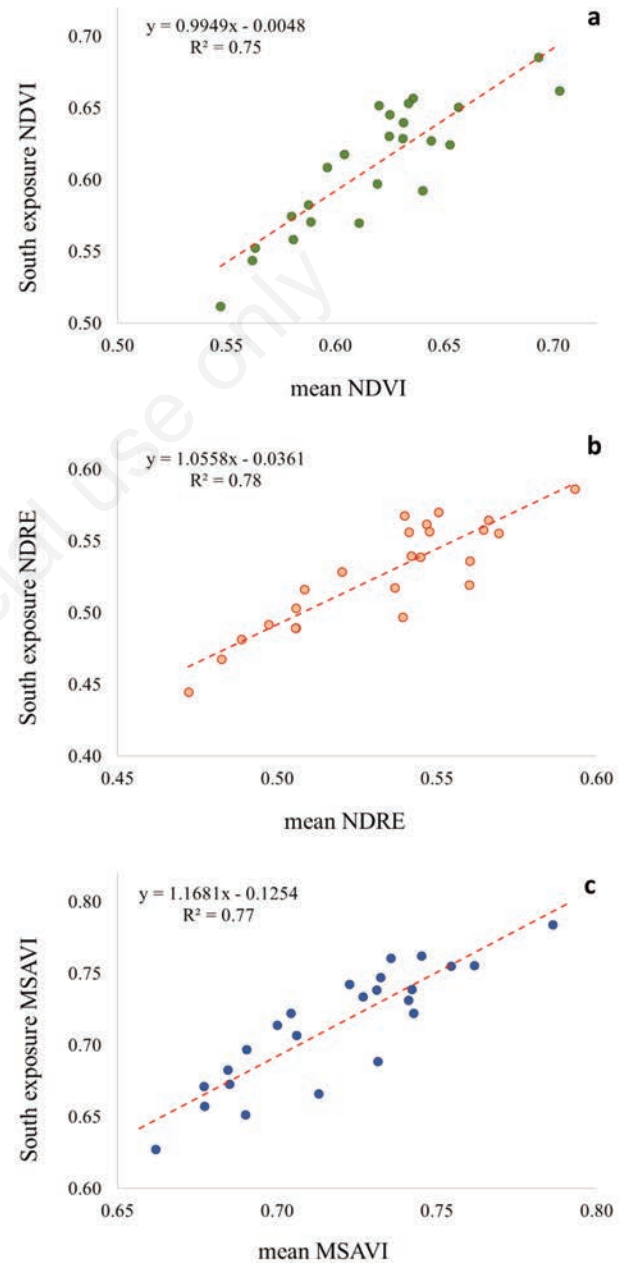


Figure 11. a) Correlation between normalized difference vegetation index values of the south exposure portion of the canopy and the mean normalized difference vegetation index value of the canopy; b) Correlation between normalized difference red-edge index values of the south exposure portion of the canopy and the mean normalized difference red-edge index value of the canopy; c) Correlation between the modified soil adjusted vegetation index values of the south exposure portion of the canopy and the mean modified soil adjusted vegetation index of the canopy.

Comparison between proximal and remote sensing data

Using the responses of the three different VI, ANOVA was applied to compare multispectral and hyperspectral data obtained by the two sensors (Figure 12). The exposure effect was statistically significant and more pronounced in the hyperspectral data than in the multispectral ones. West and South exposures gave the most consistent results with the multispectral images and the least scatter in the data for all indices used. In general, exposure had no impact on the multispectral data, unlike the hyperspectral ones. Specifically, in the South and West exposures, NDVI and MSAVI values were statistically higher than those obtained from multispectral images ($p < 0.05$). In the North and East exposures, the values were consistently lower than the ones obtained from the multispectral data for all the VI, but the high dispersion determines no difference. The best correlation between the indices calculated from the two different datasets was obtained in the southern and western exposures for all three indices. In particular, NDVI in the West exposure showed $r = 0.69^{**}$ between multispectral and hyperspectral data, while for MSAVI, the best correlation was $r = 0.63^{**}$ in the same exposure. For NDRE, the correlation between multispectral and hyperspectral data showed $r = 0.74^{**}$ in the South exposure.

Discussion

The olive tree trelling system in the experimental site is the vase shape, a traditional system with very specific peculiarities with respect to other fruit trees. The canopy, in fact, is made up of sprouts with mixed growth: procumbent and assurgent, unlike other fruit plants, which have predominantly assurgent sprouts. This peculiarity generates a canopy heterogeneously distributed in the space. The external part of the canopy has many pendulous sprouts, while the central one has an upward trend. This heterogeneous arrangement of the shoots makes the olive tree particularly interesting in studying the spectral response. The use of the two systems, therefore, allows the entire canopy to be observed from two different points of view.

The hyperspectral data are consistent with those generally found in the literature. Rubio-Delgado *et al.* (2021) have also attempted to describe and identify the spectral signature of olive trees, given the wealth of information on their health status that can be obtained. They obtained in the NIR region a slightly different curve than the one described in this study, which can be explained by the different POV of the sensor compared to the crop (Ye *et al.*, 2008). The difference in the reflectance of the hyperspectral curve in the four exposures marked the results of the entire experiment. The normalisation of the spectral data, and therefore of the calculation of the different indices, allowed a better understanding of the crop's status. The hyperspectral VI values showed a close dependence on the acquisition exposure. Nevertheless, their correlation with the multispectral data was found to be statistically significant regardless of the type of VI and exposure.

In a traditional breeding system like the one used in the experiment, the different growth conditions in the four exposures influenced the relative spectral characteristics. This effect is related to the different angles of the rows, which influences the interception of photosynthetically active radiation (PAR) (Campos *et al.*, 2017). Indeed, as observed by Campos *et al.* (2017), with the rows in the NE-SW direction, the part with the highest light interception in a latitude close to 40° are the South and West zones. In our experi-

ment, hyperspectral VI showed a clear dependence on exposure, as found in another study with hyper and/or multispectral side-view cameras (Saiz-Rubio *et al.*, 2021). The differences found among the four exposures are due to their different microclimatic conditions (temperature, relative humidity, wind). By grouping the hyperspectral data from the South and West exposures and comparing them with the North and East data, it is evident that the South-West exposure resulted in statistically higher NDVI, MSAVI and NDRE values than the North-East exposure. The higher values found in the South and West exposures can be explained by the better growing conditions of the crop due to the higher PAR values (Campos *et al.*, 2017). The result obtained in the South and West exposures is also supported by the very high and statistically

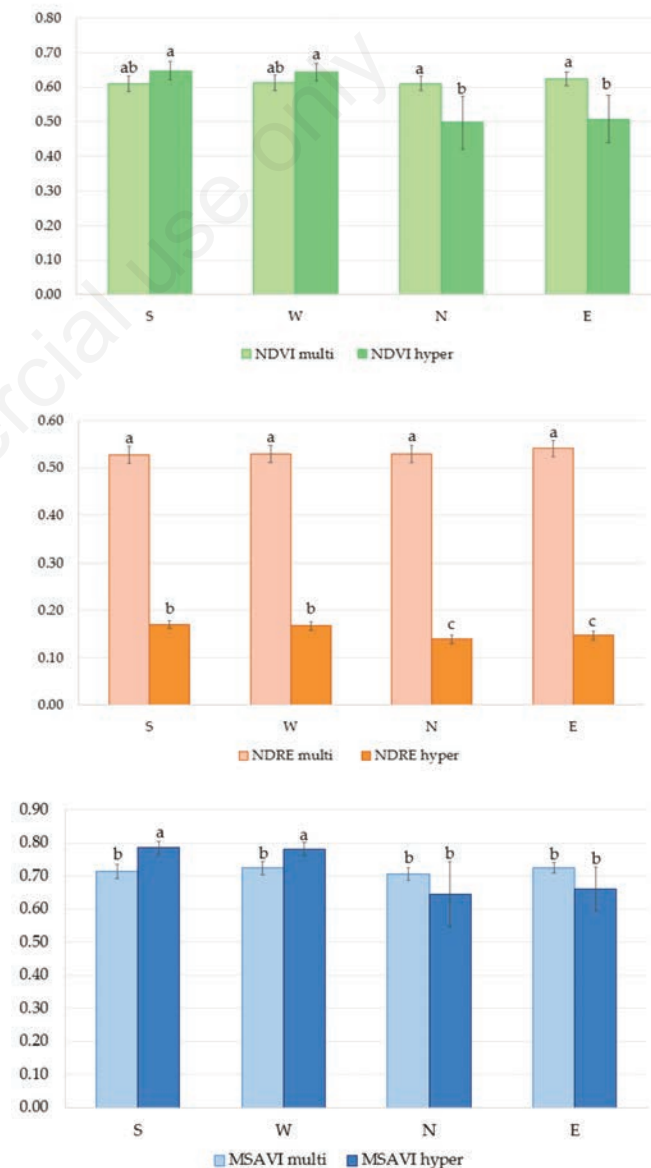


Figure 12. Normalized difference vegetation index, normalized difference red-edge index and modified soil adjusted vegetation index data calculated from multispectral and hyperspectral images for the different portions of the canopy.

significant r^2 values found between the hyperspectral and multispectral VI. It remains to be investigated how the different regions of the spectrum change and under which conditions it is correct to use one region rather than another when using side-view spectroradiometers. In fact, different studies investigated the crop status using the entire spectral signature but with more problems with the data management.

The multispectral images were able to determine for each plant the crown area and the multispectral information with high precision, as obtained in previous studies (Anifantis *et al.*, 2019; Deng *et al.*, 2018; Stateras and Kalivas, 2020). The multispectral images were thus able to appreciate the spectral condition of each plant. A good linearity of the extrapolated data was obtained from the multispectral VI analysis. In fact, no statistically significant differences were observed for the same indices among the various exposures in all three indices. However, statistically significant differences were found among all the indices, probably related to the different bands used for the calculation, thus providing different spectral information (Gómez *et al.*, 2011; Modica *et al.*, 2020).

From the comparison between multi and hyperspectral images, it can be deduced that the different VI do not associate the same value with the same level of crop stress. MSAVI generally gave higher values, followed by NDVI and then by NDRE, both from multispectral and hyperspectral data.

The use of the multi and hyperspectral sensors, despite the different viewpoints of the object, was able to describe the health status of the plants as found in Vanegas *et al.* (2018). Data from the hyperspectral camera with a side view of the object correlated well with the aerial multispectral images from the drone, paying attention to the exposure. Therefore, hyperspectral information is more accurate but at the same time more affected and/or at risk of error than multispectral information. This effect is explained by the variation in the data and the lower correlation value between the hyperspectral data in the four exposures. The exposures that showed the best correlation among the VI calculated from the two datasets were the S and W. This is probably related to the better growth conditions of the two canopy portions, confirmed by the higher values appreciable in the hyperspectral dataset, as found in (Marshall and Thenkabil, 2015).

Conclusions

The multispectral images obtained from remote sensing by drone can be compared with the hyperspectral images from proximal systems as they correlate well. This is especially the case when the proper wavelengths are used from the hyperspectral data and the acquisitions made in the South and West exposures of olive trees. The data obtained from the remote platform showed very good correlation and data matching over the whole plot and allowed investigating with reasonable accuracy. However, the possibility of obtaining spectral information from the crop, the development of new acquisition platforms from proximal sensing such as unmanned ground vehicles and the continuous improvement of technology make the use of hyperspectral sensors in precision farming increasingly interesting.

This study has shown that hyperspectral data acquired from the proximal platform with a different viewpoint can more accurately describe the crop spectral status, despite the limited diffusion of proximal sensing platforms for investigating the entire variability of the plot and the high variability of the data, depending on crop conditions as exposure and brightness. This study was able to dis-

criminate the potential of hyperspectral and multispectral data, also considering their simultaneous use. Anyway, some characteristics of the two different platforms, such as application time and data management, should be in-depth evaluated for future applications.

References

- Álamo S., Ramos M., Feito F., Cañas A. 2012. Precision techniques for improving the management of the olive groves of southern Spain. *Span. J. Agric. Res.* 583-95.
- Anifantis A.S., Camposeo S., Vivaldi G.A., Santoro F., Pascuzzi S. 2019. Comparison of UAV photogrammetry and 3D modeling techniques with other currently used methods for estimation of the tree row volume of a super-high-density olive orchard. *Agriculture* 9:233.
- Avola G., Di Gennaro S.F., Cantini C., Riggi E., Muratore F., Tornambè C., Matese A. 2019. Remotely sensed vegetation indices to discriminate field-grown olive cultivars. *Remote Sens.* 11:1242.
- Benelli A., Cevoli C., Fabbri A. 2020. In-field hyperspectral imaging: An overview on the ground-based applications in agriculture. *J. Agric. Eng.* 51:129-39.
- Ben-Gal A., Agam N., Alchanatis V., Cohen Y., Yermiyahu U., Zipori I., Presnov E., Sprintsin M., Dag A. 2009. Evaluating water stress in irrigated olives: correlation of soil water status, tree water status, and thermal imagery. *Irrig. Sci.* 27:367-76.
- Berni J., Zarco-Tejada P., Sepulcre-Cantó G., Fereres E., Villalobos F. 2009. Mapping canopy conductance and CWSI in olive orchards using high resolution thermal remote sensing imagery. *Remote Sens. Environ.* 113:2380-8.
- Campos I., Neale C.M., Calera A. 2017. Is row orientation a determinant factor for radiation interception in row vineyards? *Aust. J. Grape Wine Res.* 23:77-86.
- Caruso G., Zarco-Tejada P.J., González-Dugo V., Moriondo M., Tozzini L., Palai G., Rallo G., Hornero A., Primicerio J., Gucci R. 2019. High-resolution imagery acquired from an unmanned platform to estimate biophysical and geometrical parameters of olive trees under different irrigation regimes. *PloS one* 14:e0210804.
- Catania P., Comparetti A., Febo P., Morello G., Orlando S., Roma E., Vallone M. 2020. Positioning accuracy comparison of GNSS receivers used for mapping and guidance of agricultural machines. *Agronomy*. 10:924.
- Catania P., Orlando S., Roma E., Vallone M. 2019. Vineyard design supported by GPS application. *Int. Symp.* pp. 227-233.
- Deng L., Mao Z., Li X., Hu Z., Duan F., Yan Y. 2018. UAV-based multispectral remote sensing for precision agriculture: A comparison between different cameras. *ISPRS J. Photogramm. Remote Sens.* 146:124-36.
- Dorigo W.A., Zurita-Milla R., de Wit A.J., Brazile J., Singh R., Schaepman M.E. 2007. A review on reflective remote sensing and data assimilation techniques for enhanced agroecosystem modeling. *Int. J. Appl. Earth Observ. Geoinf.* 9:165-93.
- Er-Rami M., D'Urso G., Lamaddalena N., D'Agostino D., Belfiore O.R. 2021. Analysis of irrigation system performance based on an integrated approach with Sentinel-2 satellite images. *J. Agric. Eng.* 52.
- Gómez J., Zarco-Tejada P., García-Morillo J., Gama J., Soriano M. 2011. Determining Biophysical Parameters for Olive Trees Using CASI Airborne and Quickbird Satellite Imagery. *Agron. J.* 103:644-54.

- Gómez-Casero M.T., López-Granados F., Pena-Barragán J.M., Jurado-Expósito M., García-Torres L., Fernández-Escobar R. 2007. Assessing nitrogen and potassium deficiencies in olive orchards through discriminant analysis of hyperspectral data. *J. Ame. Soc. Hortic. Sci.* 132:611-8.
- Jensen J.R. 2009. *Remote sensing of the environment: An earth resource perspective 2/e*. Pearson Education, India.
- Jiménez-Brenes F.M., López-Granados F., De Castro A., Torres-Sánchez J., Serrano N., Peña J. 2017. Quantifying pruning impacts on olive tree architecture and annual canopy growth by using UAV-based 3D modelling. *Plant Methods.* 13:1-15.
- Kottek M., Grieser J., Beck C., Rudolf B., Rubel F. 2006. World map of the Köppen-Geiger climate classification updated.
- Lal R. 2015. 16 Challenges and Opportunities in Precision Agriculture. *Soil-Specific Farming: Precision Agriculture.* 22:391.
- Lee K.-S., Cohen W.B., Kennedy R.E., Maiersperger T.K., Gower S.T. 2004. Hyperspectral versus multispectral data for estimating leaf area index in four different biomes. *Remote Sens. Environ.* 91:508-20.
- López-Granados F., Jurado-Expósito M., Alamo S., Garcia-Torres L. 2004. Leaf nutrient spatial variability and site-specific fertilization maps within olive (*Olea europaea* L.) orchards. *Eur. J. Agron.* 21:209-22.
- Lu B., Dao P.D., Liu J., He Y., Shang J. 2020. Recent advances of hyperspectral imaging technology and applications in agriculture. *Remote Sens.* 12:2659.
- Maccioni A., Agati G., Mazzinghi P. 2001. New vegetation indices for remote measurement of chlorophylls based on leaf directional reflectance spectra. *J. Photochem. Photobiol. B: Biology* 61:52-61.
- Marin D.B., Ferraz P.F.P., Manuel P., Rossi G., Vieri M., Sarri D. 2021. Comparative analysis of soil-sampling methods used in precision agriculture. *J. Agric. Eng.* 53.
- Mariotto I., Thenkabail P.S., Huete A., Slonecker E.T., Platonov A. 2013. Hyperspectral versus multispectral crop-productivity modeling and type discrimination for the HypSIRI mission. *Remote Sens. Environ.* 139:291-305.
- Marshall M., Thenkabail P. 2015. Advantage of hyperspectral EO-1 Hyperion over multispectral IKONOS, GeoEye-1, WorldView-2, Landsat ETM+, and MODIS vegetation indices in crop biomass estimation. *ISPRS J. Photogramm. Remote Sens.* 108:205-18.
- Microsoft Corporation. 2018. Microsoft Excel. <https://Office.Microsoft.Com/Excel>.
- Modica G., Messina G., De Luca G., Fiozzo V., Praticò S. 2020. Monitoring the vegetation vigor in heterogeneous citrus and olive orchards. A multiscale object-based approach to extract trees' crowns from UAV multispectral imagery. *Comput. Electron. Agric.* 175:105500.
- Nigam R., Tripathy R., Dutta S., Bhagia N., Nagori R., Chandrasekar K., Kot R., Bhattacharya B.K., Ustin S. 2019. Crop type discrimination and health assessment using hyperspectral imaging. *Curr. Sci.* p. 116.
- Pagliai A., Ammoniaci M., Sarri D., Lisci R., Perria R., Vieri M., D'Arcangelo M.E.M., Storchi P., Kartsiotis S.-P. 2022. Comparison of Aerial and Ground 3D Point Clouds for Canopy Size Assessment in Precision Viticulture. *Remote Sens.* 14:1145.
- QGIS.org, 2022. QGIS Geographic Information System. QGIS Association, n.d.
- Qi J., Chehbouni A., Huete A.R., Kerr Y.H., Sorooshian S. 1994. A modified soil adjusted vegetation index. *Remote Sens. Environ.* 48:119-126.
- RStudio Team. 2020. *RStudio: Integrated Development for R*. RStudio, PBC, Boston.
- Roma E., Catania P. 2022. Precision Oliviculture: Research Topics, Challenges, and Opportunities - A Review. *Remote Sens.* 14:1668.
- Rouse J.W., Haas R.H., Schell J.A., Deering D.W., Harlan J.C. 1974. Monitoring the vernal advancement and retrogradation (green wave effect) of natural vegetation. *NASA/GSFC Type III Final Report, Greenbelt, Md* 371.
- Rubio-Delgado J., Pérez C.J., Vega-Rodríguez M.A. 2021. Predicting leaf nitrogen content in olive trees using hyperspectral data for precision agriculture. *Precis. Agric.* 22:1-21.
- Saiz-Rubio V., Rovira-Más F., Cuenca-Cuenca A., Alves F. 2021. Robotics-based vineyard water potential monitoring at high resolution. *Comput. Electron. Agric.* 187:106311.
- Sepulcre-Cantó G., Zarco-Tejada P., Sobrino J., Jiménez-Muñoz J., Villalobos F. 2005. Spatial variability of crop water stress in an olive grove with high-spatial thermal remote sensing imagery. *Proc. Precision. Agric.* 267-72.
- Sepulcre-Cantó G., Zarco-Tejada P.J., Jiménez-Muñoz J., Sobrino J., De Miguel E., Villalobos F.J. 2006. Detection of water stress in an olive orchard with thermal remote sensing imagery. *Agric. Forest. Meteorol.* 136:31-44.
- Sepulcre-Cantó G., Zarco-Tejada P.J., Jiménez-Muñoz J., Sobrino J., Soriano M., Fereres E., Vega V., Pastor M. 2007. Monitoring yield and fruit quality parameters in open-canopy tree crops under water stress. Implications for ASTER. *Remote Sens. Environ.* 107:455-70.
- Sghaier A., Dhaou H., Jarray L., Abaab Z., Sekrafi A., Ouessar M. 2022. Assessment of drought stress in arid olive groves using HidroMORE model. *J. Agric. Eng.* 53.
- Sola-Guirado R.R., Castillo-Ruiz F.J., Jiménez-Jiménez F., Blanco-Roldan G.L., Castro-Garcia S., Gil-Ribes J.A. 2017. Olive actual "on year" yield forecast tool based on the tree canopy geometry using UAS imagery. *Sensors.* 17:1743.
- Solano F., Di Fazio S., Modica G. 2019. A methodology based on GEOBIA and WorldView-3 imagery to derive vegetation indices at tree crown detail in olive orchards. *Int. J. Appl. Earth Observ. Geoinf.* 83:101912.
- Stateras D., Kalivas D. 2020. Assessment of Olive Tree Canopy Characteristics and Yield Forecast Model Using High Resolution UAV Imagery. *Agriculture.* 10:385.
- Sun J., Yang J., Shi S., Chen B., Du L., Gong W., Song S. 2017. Estimating rice leaf nitrogen concentration: influence of regression algorithms based on passive and active leaf reflectance. *Remote Sens.* 9:951.
- Transon J., d'Andrimont R., Maignard A., Defourny P. 2018. Survey of hyperspectral earth observation applications from space in the sentinel-2 context. *Remote Sens.* 10:157.
- Van Evert F.K., Gaitán-Cremaschi D., Fountas S., Kempenaar C. 2017. Can precision agriculture increase the profitability and sustainability of the production of potatoes and olives? *Sustainability.* 9:1863.
- Vanegas F., Bratanov D., Powell K., Weiss J., Gonzalez F. 2018. A novel methodology for improving plant pest surveillance in vineyards and crops using UAV-based hyperspectral and spatial data. *Sensors.* 18:260.
- Vanella D., Ferlito F., Torrisi B., Giuffrida A., Pappalardo S., Saitta D., Longo-Minnolo G., Consoli S. 2021. Long-term monitoring of deficit irrigation regimes on citrus orchards in Sicily. *J. Agric. Eng.* p. 52.
- Xie Q., Huang W., Liang D., Chen P., Wu C., Yang G., Zhang J.,

- Huang L., Zhang D. 2014. Leaf area index estimation using vegetation indices derived from airborne hyperspectral images in winter wheat. *IEEE J. Sel. Top. Appl. Earth Observ. Remote Sens.* 7:3586-94.
- Xue J., Su B. 2017. Significant remote sensing vegetation indices: A review of developments and applications. *J. Sens.* 2017.
- Ye X., Sakai K., Okamoto H., Garciano L.O. 2008. A ground-based hyperspectral imaging system for characterizing vegetation spectral features. *Comput. Electron. Agric.* 63:13-21.
- Zhang C., Valente J., Kooistra L., Guo L., Wang W. 2021. Orchard management with small unmanned aerial vehicles: A survey of sensing and analysis approaches. *Precis. Agric.* 22:2007-52.
- Zhang N., Wang M., Wang N. 2002. Precision agriculture - a worldwide overview. *Comput. Electron. Agric.* 36:113.32.

Non-commercial use only